Chapter 20
Effective Drying Zones and Nonlinear Dynamics in a Laboratory Spray Dryer

Ulises Ramón Morales-Durán, Liliana Alamilla-Beltrán, Humberto Hernández-Sánchez, Jose Jorge Chanona-Pérez, Antonio Ruperto Jiménez-Aparicio, and Gustavo Fidel Gutiérrez-López

20.1 Introduction

Extensive experimental spray drying tests have been carried out by various researchers to assess drying kinetics inside the chamber (Zbicinski et al. 2002). At the beginning of this decade, about 20,000 spray dryers were used commercially for processing agrochemical, biotechnological, chemical, pharmaceutical, and food products. Evaporative capacities of spray drying equipment are in the range of 1–10 L/h for laboratory units and up to about 200 t/h for large-scale processing (Mujumdar and Devahastin 2000). Use of inadequate drying systems and incorrect drying conditions may lead to obtaining products in which added value and physical and chemical properties do not meet the required specifications. Also, in some cases, deposition of wet or rubbery product on the wall of the drying chamber may occur, causing enormous economical losses (Goula and Adamopoulos 2004). Selecting drying conditions, atomizing device, and size and geometry of the drying chamber must take into account the desired characteristics of the product and, in most cases, involve complex mass and heat transfer calculations. The most common food powders are baby foods, dairy products, proteins, coffee and tea extracts, flavors and encapsulated fats (Chen and Patel 2008; Goula and Adamopoulos 2008). The amount of moisture removed from a droplet inside the drying chamber depends on the mechanisms that govern the evaporation rate and the residence time of the droplet in each zone of the equipment. This phenomenon can be described using transport equations, CFD (Seydel et al. 2006; Zbicinski and Li 2006) and nonlinear considerations (Van den Bleek et al. 2002).

U.R. Morales-Durán, L. Alamilla-Beltrán, H. Hernández-Sánchez, J.J. Chanona-Pérez, and G.F. Gutiérrez-López (✉)
Departamento de Graduados e Investigación en Alimentos, Escuela Nacional de Ciencias Biológicas, Instituto Politécnico Nacional, Carpioy Plan de Ayala, s/n CP. 11340, México DF, Edomex, Mexico
e-mail: gusfgl@gmail.com

A.R. Jiménez-Aparicio
Carretera Yautepec-Jojutla, Km. 6, calle CEPROBI No. 8, Col. San Isidro, Yautepec, Morelos, C.P. 62731, México

Some authors consider that atomization is a key stage in the process (Allen and Bakker 1994; Furuta et al. 1994; Oakley 1994). Type of atomizer and feed partially determine the kind of drying chamber to be used and the energy spent in atomizing. Size distribution of the spray as well as particle trajectory and velocity inside the chamber and powder collection system will also contribute to the overall quality of the operation (Filoková and Mujumdar 1995; Chawla 1994). Moreover, in some cases particles can produce turbulence, which in time can lead to different rates of transport that may affect the quality of the product using the same equipment (Van den Bleek et al. 2002).

Special attention should be given to drying times, trajectories of particles, and the time that droplets take to reach the wall of the dryer. Chamber diameter and volume play a key role regarding this issue (Gutiérrez et al. 1997, 1998). Droplets of variable size and different morphology should reach the wall and leave the dryer at the desired final moisture content. For certain foods, drops in spray dryers often approach and reach the boiling temperature of the dissolvent (water in most food related applications); vapor generation may cause particles to grow in size and then collapse. Bubbles may form and collapse repeatedly in a process known as morphological development (Hecht and King 2000). The complexity of the spray drying process makes experimental study of mass transfer from individual drops impractical, which has induced research on predicting moisture content as well as on morphological characteristics of particles during the process by suspending a drop of the material under study in a fixed position (Adhikari et al. 2000; Ferrari et al. 1989). In this context, digital image analysis can play an important role when evaluating changes in particle size, formation of crust, shrinkage, inflation, blow-up, presence of holes, etc. (Adhikari et al. 2000; Aguilera and Stanley 1999). Reports on the prediction of various thermal and hydrodynamic conditions have made it possible to distinguish among different phenomena associated with droplet morphology and have allowed the recognition of periods and actual drying zones in drying chambers (Dolinsky 2001).

Identification of drying zones inside the chamber and change of moisture content during dehydration may help to establish relationships between dryer design and product quality. In this work, effective drying zones evaluated as heat transfer units in the chamber as well as the morphological development of the particle using digital image analysis are reported for a two-fluid nozzle laboratory co-current spray dryer. Also, computational fluid dynamics (CFD) has been used in this work to evaluate hydrodynamics to assess the effects of particle-gas interactions in the effective drying zones. This has allowed the establishment of correlations between lumped models and nonlinear considerations of air-particle interactions, including the evaluation of Lyapunov coefficients and formation of attractors for trajectories (Van den Bleek et al. 2002). Computer vision systems may be applied to aid discussion of the usefulness of traditional design calculations and findings derived from intensive computing exercises, as well as from advanced theories on chaotic behavior.

20.2   Materials and Methods

20.2.1   Testing Material

Testing material was, in all cases, 40% TS maltodextrin solution (20 ED) supplied by Arancia Corn Products S.A. (Mexico). Experiments on trajectories of particles were performed by using powdered maltodextrin (20 ED) supplied by the same company.

20.2.2   Spray Dryer

The spray dryer used in this work was a two-fluid nozzle co-current laboratory spray dryer equipped with a peristaltic pump for feed fine control and cyclone for powder collection. The dryer is depicted in Fig. 20.1. The dimensions of the drying chamber were diameter 0.38 m, height 0.60 m, and height of cone 0.40 m. Details of design and construction of the experimental dryer are given elsewhere (Alamilla-Beltrán et al. 2001). The evaporative capacity of the dryer is 0.8 kg of evaporated
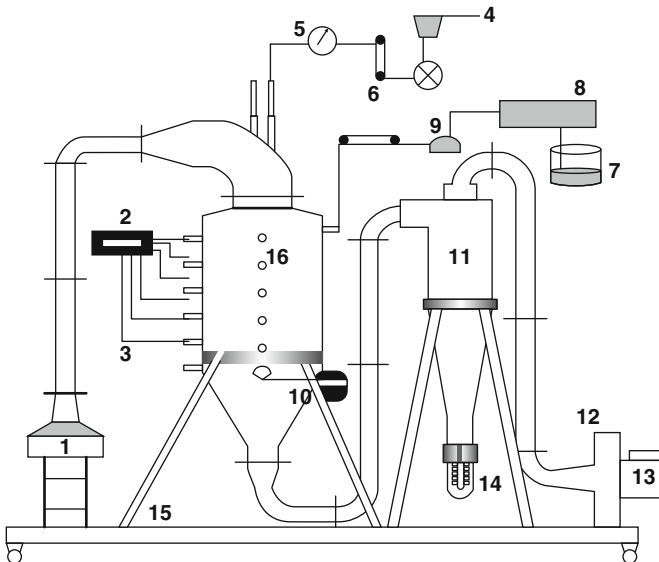

Fig. 20.1 Diagram of spray dryer. (**a**) Heater; (**b**) temperature recorder; (**c**) thermocouples; (**d**) air to nozzle; (**e**) manometer; (**f**) rotameter; (**g**) liquid feed; (**h**) feed pump; (**i**) pulse dampener; (**j**) thermoanemometer; (**k**) cyclone; (**l**) fan; (**m**) motor; (**n**) powder collector; (**o**) supporting structure; (**p**) drying chamber

water/h (similar to laboratory-scale dryers, e.g., SDMicro^{TM} Spray Dryer, Niro; Mini Spray Dryer B-290, Büchi).

Experiments were conducted under the following drying conditions: inlet/outlet temperatures of 200/173°C (denoted as high-temperature drying), and 170/145°C (denoted as low-temperature drying) and volumetric airflow of 75 m³/h. Feed rate was, in all cases, 1.39 kg/h. The nozzle was located at 0.1 m from the top of the chamber. A J-type thermocouple was used to measure the inlet air drying temperature. At the bottom of the chamber the outlet air drying temperature was evaluated.

20.2.3   Moisture Content and Sampling of Material

Sampling of material inside the chamber was performed using a bayonet-type sampler previously described (Alamilla-Beltrán et al. 2005). It was introduced to the dryer through specially constructed tapped devices separated 0.10 m from each other. A diagram of the dryer showing the measuring points is presented in Fig. 20.2. Average moisture content was evaluated following AOAC 32.1.03 method (AOAC 1995) for the different heights of the chamber in which each sample was collected. Sampling was performed once drying proceeded in a constant regime.
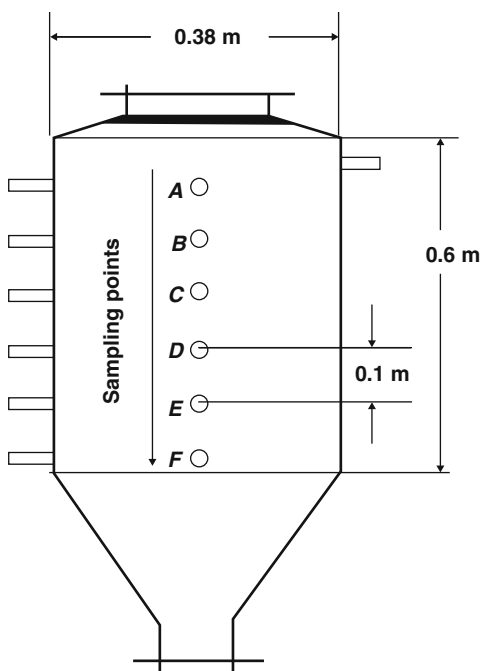

Fig. 20.2 Diagram of the longitudinal section of the dryer showing sampling points and chamber dimensions

20.2.4 Evaluation of Air and Product Temperature

The air drying temperature was evaluated using thermocouples type J. One thermocouple was fitted at the air inlet. A second thermocouple was positioned at the air outlet duct at the bottom of the chamber. This thermocouple was used to measure the outlet air drying temperature. The thermocouples were adapted to a digital register, Barnant (model 692). The wet bulb temperature was measured at the same points and inside the chamber at the sampling points (Fig. 20.2) during the drying process. With dry bulb temperature and wet bulb temperatures, the enthalpy was calculated. The product temperature was measured using the thermocouple collocated at the sampling point A.

20.2.5 Mean Particle Diameter During Drying

Particles obtained during drying experiments were observed using light microscopy. The microscope (Zeiss Axiophot) was fitted with a $20\times$ objective and blue filter (total magnification $100\times$ and $200\times$, depending on drying experiment). The illumination was provided by a light-field source. Images were obtained by means of a digital camera (ZVS-47DE) with resolution of 640×480 pixels and captured in a PC. KS400 ver. 3.01 software was used to process images and to determine the diameter of individual particles. Mean diameter of particles at different heights in the chamber was reported as the corresponding average value for powders collected at the center of the spray-cone and at different heights along the drying chamber as depicted in Fig. 20.2. Initial diameter of the droplet was measured using a particle analyzer Malvern Series 2,600 at the feed rate and atomizing air pressure used in the drying operation.

20.2.6 Measurement of the Mass Flow Rate

Mass flow rate of air (Gs) was evaluated by measuring the mean air velocity in the air exhaust duct of the dryer with a hot-wire anemometer (Digital Thermoanemometer TSI Inc., model 8330-M, USA). Mass flow rate of liquid (L) was evaluated using a peristaltic pump (Masterflex-Cole Parmer Instrument, model 7521–40). Spraying air was controlled by means of a rotameter (Blue White).

20.2.7 Effective Drying Height

In this work, a proposal for the calculation of the effective drying height based on the application of transfer units was applied. This methodology considers that the longitude along which one of the fluids travels through the dryer is formed

by the number of transfer units (N_{tOG}) corresponding to a dimensionless function of the difference of temperatures and the driving force for heat transfer. The height of the transfer unit (H_{tOG}) is a function of the conditions of flow.

The evaluation of the effective drying height was based on the consideration that the drying process is similar to the humidification operation, with the exception of the influence of the solids (Foust et al. 1993). This influence is important and in this proposal it was considered that the drying air is humidified in adiabatic form during the process. The flow diagram for the proposal is presented in Figs. 20.3 and 20.4. Figure 20.3 illustrates calculations of the product temperature at different points along the dryer, and Fig. 20.4 shows the evaluation of the effective drying height.

The number of transfer units is related to its capacity to transfer heat and may be evaluated by using (20.1).
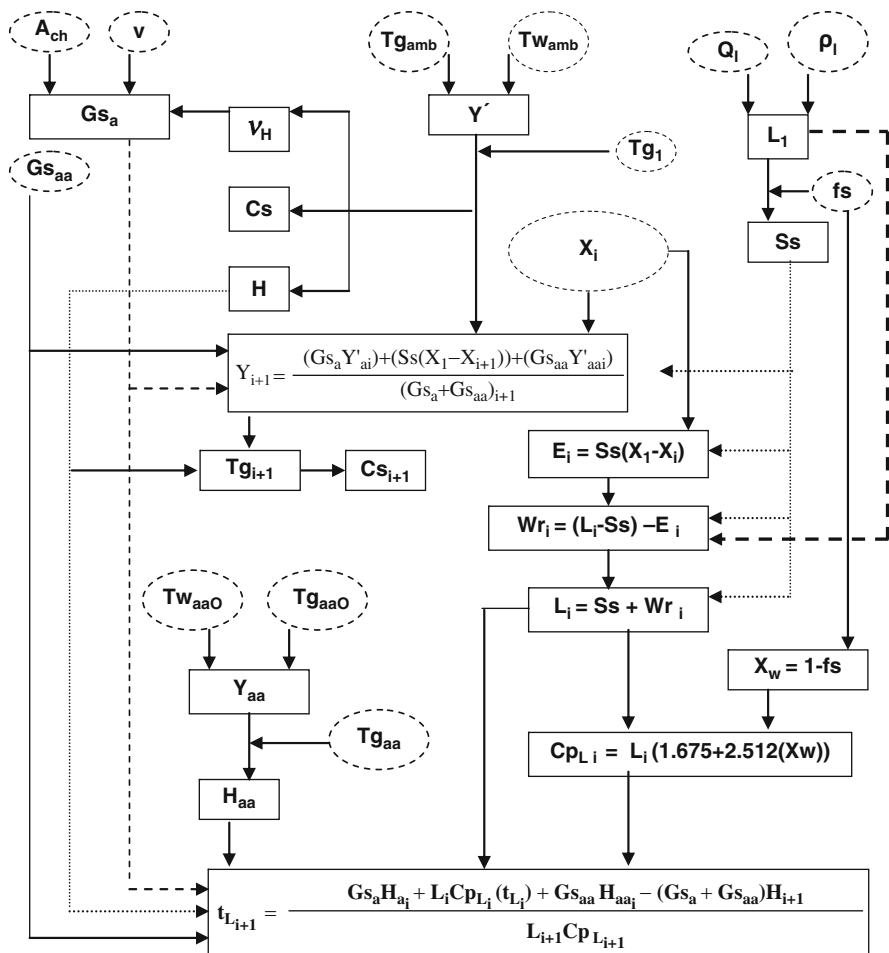

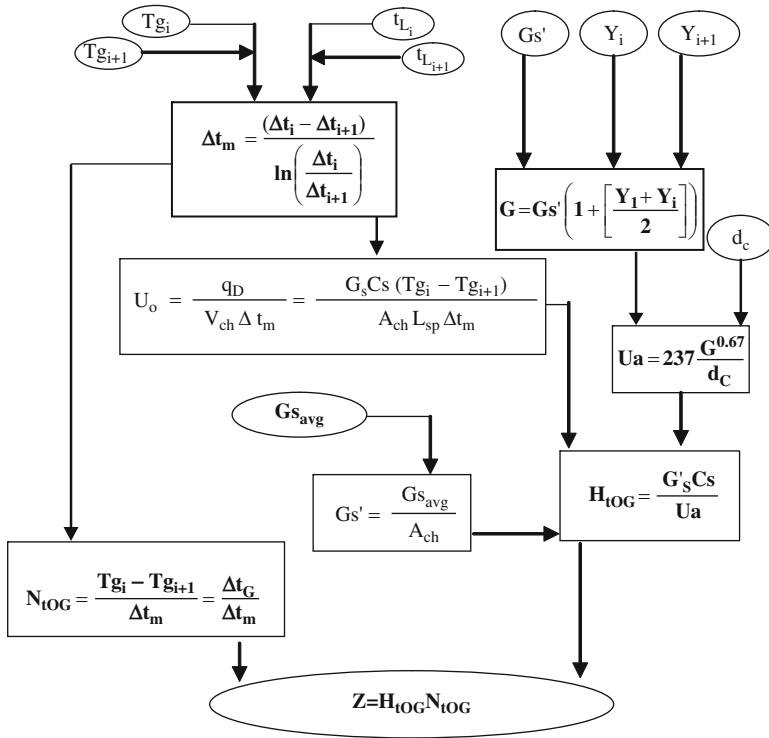**Fig. 20.3** Flow diagram of evaluation of product temperature

Fig. 20.4 Flow diagram of evaluation of effective drying height

The height of the heat transfer unit depends on the volumetric coefficient of heat transfer and the volumetric airflow. It can be calculated as follows (Treybal 1996):

$$N_{\text{tOG}} = \frac{Tg_i - Tg_{i+1}}{\Delta t_m} = \frac{\Delta T_g}{\Delta T_m} \tag{20.1}$$

In the case of rotational dryers (in which air flows through a mass of dispersed solids), the volumetric coefficient of heat transfer in kJ/(h) (m³ of dryer) (°C) can be calculated with (20.3). This equation is based on the flow mass of drying air by unit of transversal area, and the diameter of the same one (Friedman and Marshall 1949; McCormick 1962).

$$H_{\text{tOG}} = \frac{G'_s C_s}{\text{Ua}} \tag{20.2}$$

An increase in the speed of the gas will increase the exposed surface. The contact air-particle consists of a mass of humid material in dispersed phase in contact with drying air in the continuous phase.

$$\mathrm{Ua} = 237 \; \frac{G^{0.67}}{d_{\mathrm{c}}} \tag{20.3}$$

The number of transfer units and the length of a transfer unit are related by means of (20.4) (Treybal 1996). This relationship allows determination of the value of the effective drying height (Z) inside the drying chamber.

$$Z = N_{\mathrm{tOG}} \, H_{\mathrm{tOG}} \tag{20.4}$$

20.2.8 Computational Fluid Dynamics Simulation

Simulation of the drying process was carried out using CFX 10.0. Drying air velocity field was simulated using the k–ε (Southwell and Langrish 2000; Langrish et al. 2004). The Lagrangian–Euler approach was selected for the resolution of the discrete phase. Drag force was assessed using the Schiller–Nauman correlation. Airflow and particles-air interactions were also evaluated.

20.2.9 Simulation of Airflow Profiles

To simulate the air-velocity of drying air, a three-dimensional representation of the equipment was made. Domain was divided in a 138,717 elements. Boundary conditions were established, with inlet air taken as 1.54×10^{-2} kg/s according to experimental data. Atomizing air inlet was 116 m/s corresponding to 1.54×10^{-4} kg/s evaluated by considering the flow divided by the area of annulus of the nozzle. At the outlet zone of the dryer, a relative static pressure of 0 Pa was considered. A steady-state simulation was carried out until reaching an average relative error of 10^{-4}. Steady-state simulation was used as the initial value of nonsteady-state flow for 10 s, using a 0.24 s resolution. The need for these sorts of experiments and CFD simulation has been noted by Fletcher et al. (2006).

20.2.10 Nonlinear Dynamics of the System

Dynamics of a dispersed maltodextrin powdered phase in the chamber was evaluated under airflow drying conditions. Fifty grams per minute of powdered maltodextrin having a range of particle sizes of 5–45 μm was fed into the dryer. A 200 mW laser beam was fitted to the dryer to axially illuminate the trajectories of the particles. Images of the trajectories were taken using a webcam (iSlim 2020 AF. Genius, USA) every 0.24 s. Images were taken at 0.1 m and 0.3 m from the

atomizing nozzle in the axial direction, which also corresponded to air velocity-measuring points. Crops of images were obtained and fractal dimension of texture (FDT) was evaluated by using the SDBC plugging of ImageJ (Chen et al. 2003). Series 2 min long were recorded to observe oscillations of the FDT values. Time series so obtained were processed to derive the corresponding Lyapunov coefficients of the system and the phase-space of reflected light (Wolf et al. 1985). These calculations could render useful information on the nonlinear (chaotic) behavior of the system and allow the derivation of important conclusions on overall tendencies of flow into the dryer by calculating Kolmogorov Entropy values.

20.3 Results and Discussion

Evaluation of the number of transfer units allowed recognition of the three different stages during drying. The experimental evidence of water removed from the product (moisture content), temperatures of the drying air and the product (inside the aspersion cone), along with changes in particle size (shrink and expansion) have been associated with the stages of drying. Two of these factors are related to water evaporated and shrinkage and a third with particle growth.

Initially, a first zone called the first drying stage was observed, in which elimination of water solely occurs without the generation of powder. It would be possible to assume that the flow in drying zones is less mixed than for zone 3 (or that a controlling flow induced by the nozzle is generated). This section coincides with the characteristics of stages I and II as reported by Dolinsky (2001).

A second zone, called the second drying stage was observed in which the formation of the shell of the particle generates a powdered product with almost the equivalent of the final moisture of the solid. For the low-temperature operation, a 93% loss of moisture was reached, while for high-temperature drying, the loss of total humidity was 97%. In both cases, the temperature of the air reached minimum value. Also, shrinkage of the particle was observed along with an incipient expansion. At 200°C, particles shrank, mainly within the spraying cone. This could not be appreciated at 170°C, but it is probable that similar phenomena would be observed between 0.2 m and 0.3 m below the nozzle. At the same time, the temperature of the product increased from the adiabatic-saturation temperature until the boiling temperature of water was reached. Likewise, in this stage, the volumetric coefficient of heat transfer had the highest value, suggesting the existence of a pattern of mixed-flow. This section agrees with the characteristics of the stage III reported by Dolinsky (2001). A better description of this mixed-flow can be carried out by applying CFD techniques such as those described in the Materials and Methods section.

After the drying stages, a third zone, denominated as the expansion stage was detected. In this phase it was observed that after shrinkage the particle begins to expand. The size of the particle increased twofold and occasionally presented cracking, and in some cases, explosion of the material and rupture of the shell were observed. Particles that exploded were, in general, hollow spheres presenting

thin crusts for high-temperature drying conditions and thick crusts for low-temperature drying conditions. The presence of this stage is related to the temperature of the drying air, the moisture of the particle, and the gradient of pressures between the interior and the exterior of the droplet. In this zone, the loss of humidity was not significant and it could be considered as not important for drying. Also, in this zone, the temperature of the solid remained constant at its higher value. In this stage, the volumetric coefficient of heat transfer presented its lower value. Stages IV and V as reported by Dolinsky (2001) coincide with this expansion stage. The effective height of drying represents the minimum longitude to carry out effective drying.

On the other hand, solids concentration of the feed, inlet air drying temperature, mass flow of inlet product, mass flow of atomizing air, and type of feed can modify the morphological development of the particle and, in consequence, the final characteristics of the product. Changes in operating conditions will cause different effective heights of drying. However, drying and expansion stages will be present for this material. In Figs. 20.5 and 20.6, a pictorial representation of punctual temperatures of air and images of the product are presented for both experimental conditions. The shadowed areas represent each of the recognized drying stages.

In Fig. 20.7 a representation of nonsteady-state air patterns inside the chamber is presented. No influence of the nozzle in this case was considered. It should be noted that there is a recirculating airflow with a central downward jet similar to a flow in an infinite plenum surrounded by an upward stream of air. The highest density of upward flow vectors was found in the first and part of the second drying zone corresponding to the effective drying zones evaluated earlier through the evaluation
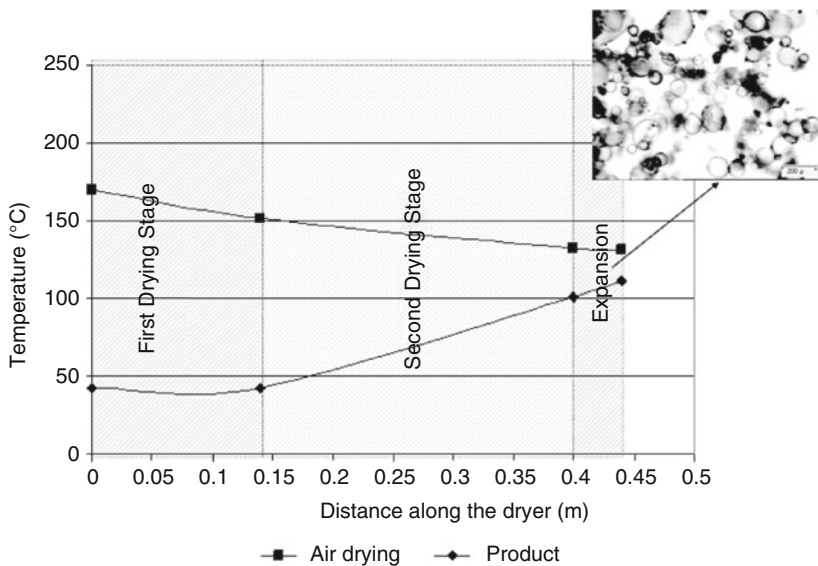

Fig. 20.5 Temperature profile of drying air and product inside the dryer and an image of the final dried product, corresponding to the condition 170/145°C
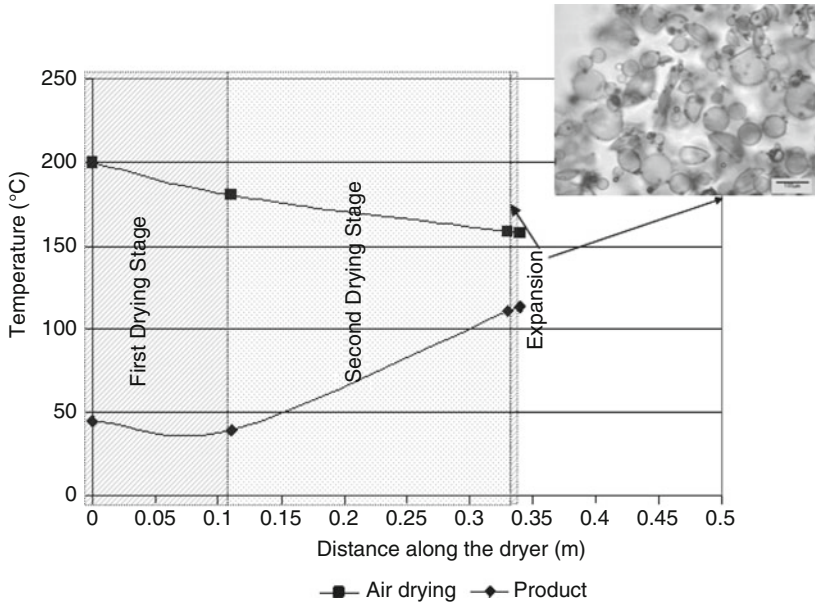
Fig. 20.6 Temperature profile of drying air and product in the dryer and an image of the final dried product, corresponding to the condition 200/173°C
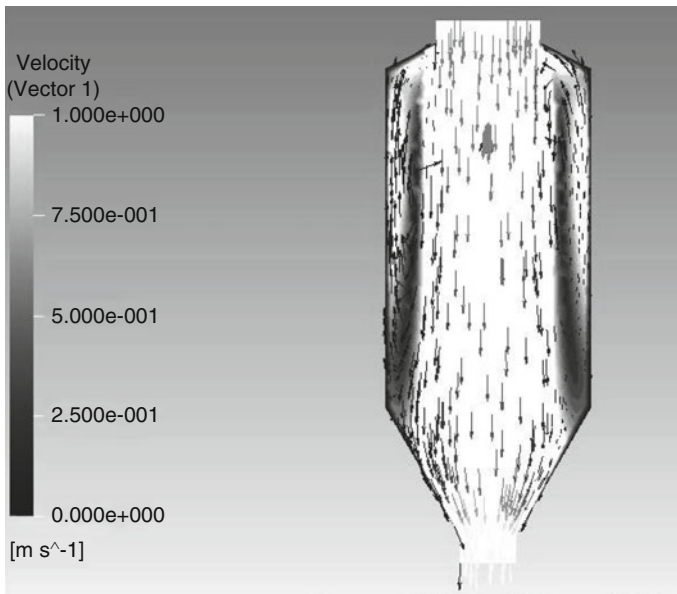

Fig. 20.7 CFD representation of non steady-state air patterns inside the chamber with no influence of the nozzle

of the transfer units, which may explain the intense drying in this region. In Fig. 20.8, the representation of nonsteady-state air patterns with influence of the nozzle is presented at different times of simulation. It is possible to observe that a nonstable air pattern was found. However, in all cases, a denser zone of mixed

Fig. 20.8 Representation of nonsteady-state air patterns with influence of the nozzle presented at 0, 5, and 10 s of simulation
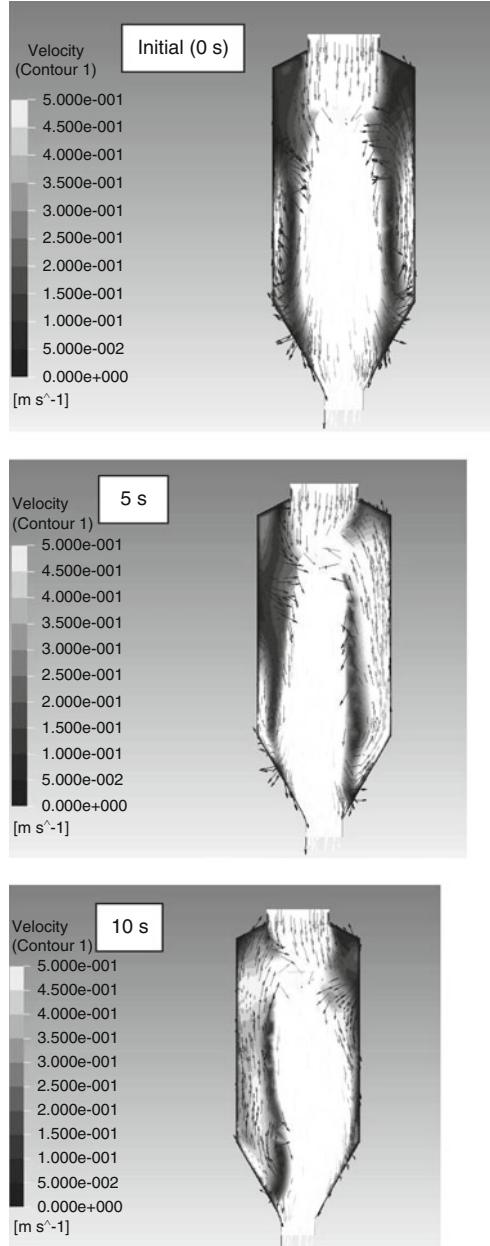
(upward and downward) flow was found, which confirms that effective drying zones are found in the first zone (first and second drying zones) of the chamber.

In Fig. 20.9, it is possible to observe the simulated trajectories of the particles used as tracers with no influence of the atomizing nozzle. Most particles were directed to the bottom of dryer since drag dominated the process. However, when the nozzle was considered in the simulation (Fig. 20.10), an imbalance of trajectories was caused and the nozzle governed hydrodynamics. This phenomenon was validated experimentally by feeding particles to the drying chamber. Images of an air-particles mix were taken by illuminating the field with the laser beam. Reflected light was scattered and seemed to present irregular patterns that were evaluated by calculating their fractal dimension at different times. Surface 3.D plots of gray-level intensity are shown in Fig. 20.11; they show the heterogeneity of laser beam reflection in the particles and are an indicator of oscillation of the air-particle flow. FDT was presented in the form of phase-space graphs, and the formation of attractors was evident. For 10 cm axial distance from the top, Lyapunov coefficients in the range of 3.46–13.62 were obtained, while for 30 cm the coefficients were
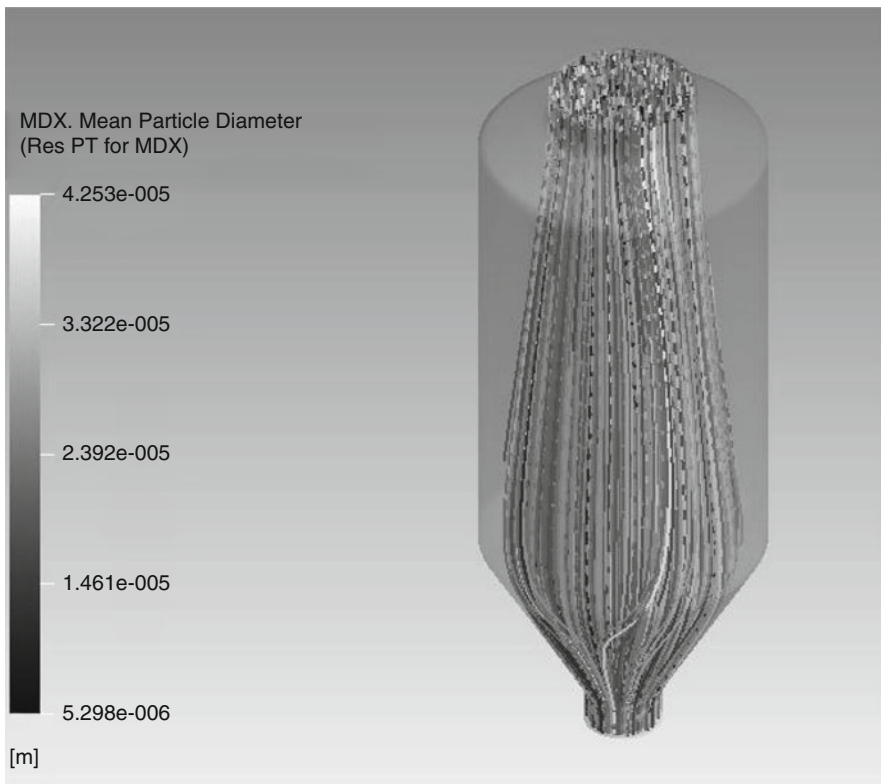

Fig. 20.9 Simulated trajectories of the particles used as tracers with no influence of the atomizing nozzle; most particles were directed to the bottom of the dryer since drag dominated the process
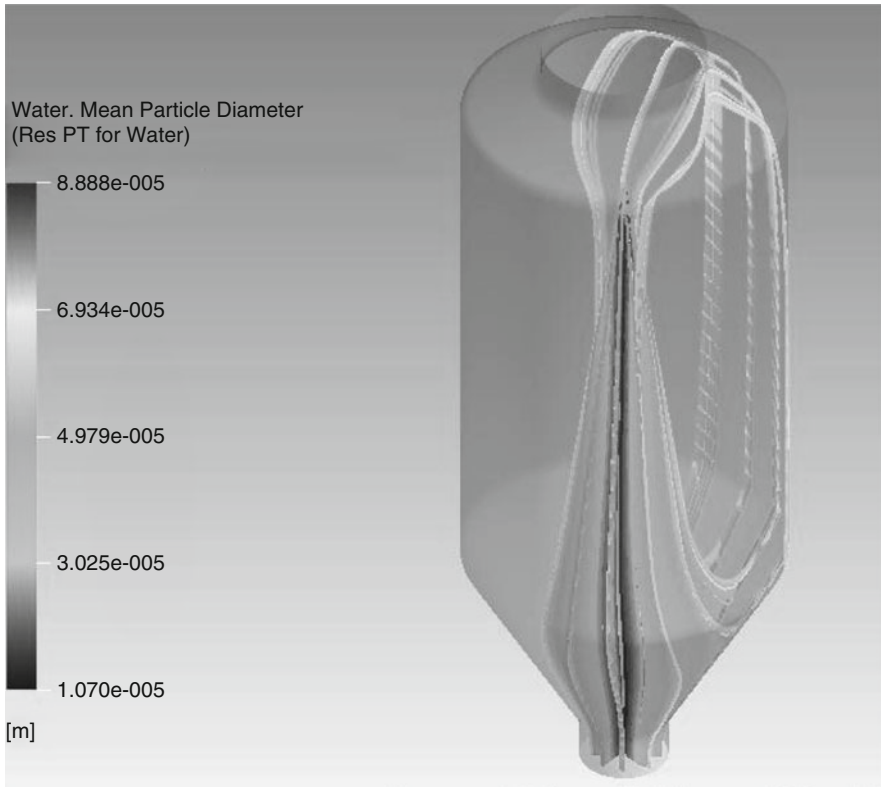
Fig. 20.10 Simulated trajectories of the particles used as tracers with the presence of the atomizing nozzle showing an imbalance of trajectories

5.44–11.63. These results also confirmed that more turbulent zones are found around the atomizer and within the first drying zone evaluated earlier through the evaluation of the transfer units, which may explain the intense drying in this region. These results also agree with those obtained by Huang et al. (2005) who used a k–ε model and found that the highest turbulence was around the atomizing device. In Figs. 20.12 and 20.13, graphs on the oscillations of FDT and corresponding Lyapunov coefficients are presented, as well as phase-space diagrams showing the obtained attractors at 10 and 30 cm axial distance from the top of the dryer.

20.4   Conclusions

The application of the concept of the number of transfer units in spray drying allowed the establishment of three stages related to the drying of the material. An initial first drying stage was identified, in which the product temperature remained
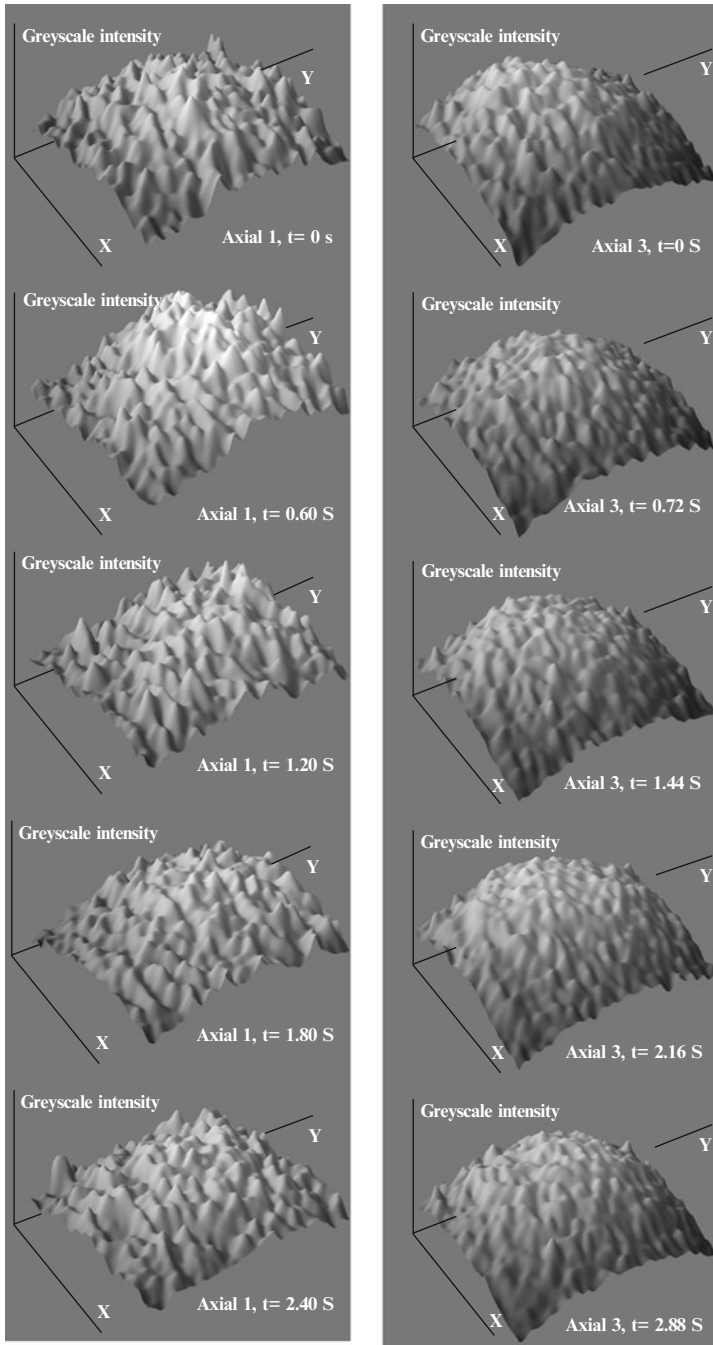
Fig. 20.11 Surface 3-D plots of gray-level intensity corresponding to laser beam reflection on particles, showing heterogeneity of flow at: (**a**) 10 cm and (**b**) 30 cm axial distance from the nozzle
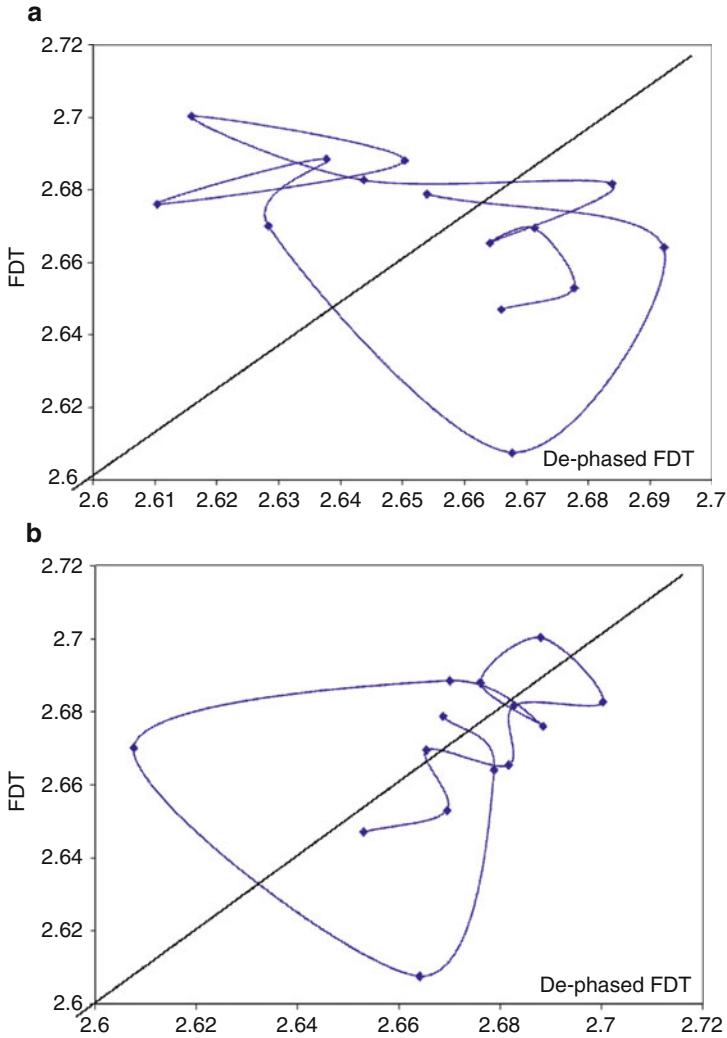
a

b

Fig. 20.12 Phase-space diagrams of FDT showing the presence of an attractor at: (**a**) 10 cm and (**b**) 30 cm axial distance from the nozzle. The 45° straight line shows the nearest neighboring points

constant and near to the adiabatic saturation temperature of the drying air. A second drying stage was identified, which showed an increase in the product temperature with the presence of dry powder. A third expansion stage was then identified in which an increment in the size of the particle was observed. The first and second drying stages represent the area in which an effective drying inside the spraying chamber was carried out. The calculated values of the volumetric coefficient of heat transfer allowed the assumption that in the second drying stage a pattern of mixed
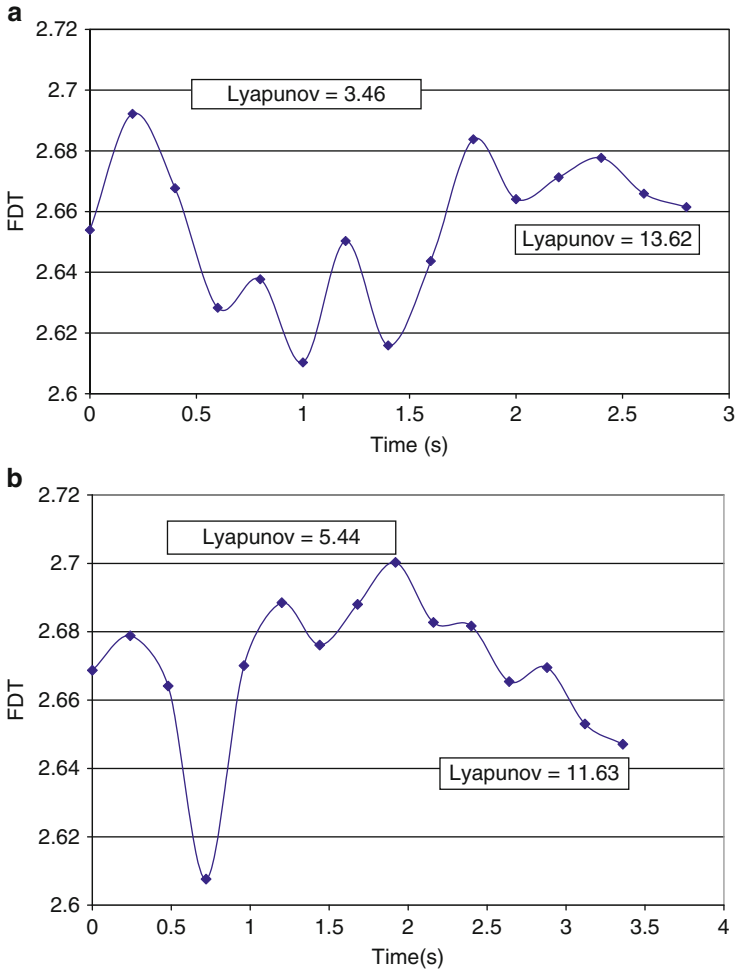
Fig. 20.13 Oscillations of FDT and corresponding Lyapunov coefficients for: (**a**) 10 cm and (**b**) 30 cm axial distance from the nozzle. Distance of text-box covers points used for calculation

flow was present. Drying zones presented according to CFD simulation (and experimental validation) a high deal of air-particle recirculation phenomena. Nonlinear dynamics could characterize these recirculation zones by using Lyapunov coefficients and by the presence of attractors related to fractal dimension of texture of the reflected laser beam cropped images. Highest simulated and validated turbulence was found in the upper part of the dryer. Steady and nonsteady-state simulations allowed insight into the nonlinear properties of generated turbulence. While the transfer units approach is useful for construction of lumped models, CFD and experiments based on air-particle trajectories constitute a good approach for the

understanding of turbulence inside the dryer. Both approaches may be useful and could complement each other for design purposes.

20.5 Symbols

A_{ch} Chamber area (m)
Cp_L Heat capacity of liquid
C_s Heat capacity of moist air (kJ/kg°C)
E   Mass flow rate of water evaporated (kg of water/h)
F_s Fraction of solids
Gs   Mass flow rate of air (kg/h)
Gs′   Mass flux of air (kg/h m^2)
Gs_m Average mass flow rate of air
H   Enthalpy of air (kJ/kg of dry air)
H_{tOG} Length of heat-transfer units (m)
L   Mass flow rate of liquid (kg/h)
L_{sp} Distance between sampling points (m)
N_{tOG} Number of heat-transfer units
Q_l Volumetric flow rate of liquid (m^3/h)
q_D Rate of heat flow (kJ/h)
t_L Temperature of the solution or dry solid (°C)
T_g Temperature of drying air (°C)
T_w Wet bulb temperature of drying air (°C)
Uo   Volumetric heat transfer-coefficient (kJ/h m^{3}°C)
Uo_m Average volumetric heat transfer-coefficient (kJ/h m^{3}°C)
v   Air velocity (m/s)
V_{ch} Volume of cylindrical section of the spray chamber (m^3)
v_h Humid volume (m^3/kg dry air)
Wr   Water in the solution (kg of water/h)
X   Moisture content (dry basis) (kg of water/kg of dry solid)
Xw   Moisture content (wet basis) (kg of water/kg of solution)
Y   Absolute humidity of air (kg of water/kg of dry air)
Z   Effective length of drying, m

20.5.1 Greek Letters

Δt   Temperature difference between air and dry solid or solution (°C)
$Δt_G$ Change in gas temperature owing to heat transfer to solid only (°C)
$ρ_l$ Density of liquid (kg/m^3)
$Δt_m$ Logarithmic-mean temperature difference (°C)
ω   Dry solid

20.5.2   Subscripts

1   At the inlet conditions of spray dryer
2   At the outlet conditions of spray dryer
aa   Atomizing air
aa_O Atomizing air at ambient conditions
amb   Ambient
a   Drying air
i   Sampling point, inlet conditions of spray dryer

References

Adhikari B, Howes T, Bhandari B, Truong V (2000) Experimental studies and kinetics of single drop drying and their relevance in drying of sugar-rich foods: a review. Int J Food Prop 3(3):323–351

Aguilera J, Stanley D (1999) Simultaneous heat and mass transfer: Dehydration. In: Microstructural principles of food processing and engineering, 2nd edn. Aspen Publishers, New York, pp 373–411

Alamilla-Beltrán L, Hernández-Parada A, Chanona-Pérez J, Jiménez-Aparicio A, Suárez-Fernández O, Santiago-Pineda T, Gutierrez-Lopez G (2001) Design and performance of a spray dryer for food processing. Proceedings of the 8th International Conference on Engineering and Food. ICEF 8, Technomic Pub. Co, USA, pp 1151–1155

Alamilla-Beltrán L, Chanona-Pérez J, Jiménez-Aparicio A, Gutiérrez-López G (2005) Description of morphological changes of particles along spray drying. J Food Eng 67(1–2):179–184

Allen R, Bakker H (1994) Spray dryer control-based on line particle size analysis. Trans IChemE Part A: Chem Eng Res Design 72:251–254

AOAC (1995) Official methods of analysis of AOAC International, 16th edn. AOAC International, USA, pp 31–32

Chawla J (1994) Effect of the droplet agglomeration on the design of spray dryer towers. Drying Technol 12(6):1357–1365

Chen X, Patel K (2008) Manufacturing better quality food powders from spray drying and subsequent treatments. Dry Technol 26(11):1313–1318

Chen W-S, Yuan S-Y, Hsieh C-M (2003) Two algorithms to estimate fractal dimension of gray-level images. Opt Eng 42(8):2452–2464

Dolinsky A (2001) High-temperature spray drying. Dry Technol 19(5):785–806

Ferrari G, Meerdink G, Walstra P (1989) Drying kinetics for a single droplet of skim milk. J Food Eng 10:215–230

Filoková I, Mujumdar A (1995) Industrial spray drying systems. In: Mujumdar A (ed) Handbook of spray drying. Marcel Dekker, New York, pp 263–307

Fletcher D, Guo B, Harvie D, Langrish T, Nijdam J, Williams J (2006) What is important in the simulation of spray dryer performance and how do current CFD models perform? Appl Math Model 30(11):1281–1292

Foust A, Wenzel L, Clump C (1993) Principles of unit operations. CECSA, México

Friedman S, Marshall W Jr (1949) Studies in rotary drying. Part II – heat and mass transfer. Chem Eng Prog 45(9):573–588

Furuta T, Hayashi H, Ohashis T (1994) Some criteria of spray drying design for food liquid. Dry Technol 12(1–2):151–177

Goula A, Adamopoulos K (2004) Influence of spray drying conditions on residue accumulation: Simulation using CFD. Dry Technol 22(5):1107–1128

Goula A, Adamopoulos K (2008) Effect of maltodextrin addition during spray drying of tomato pulp in dehumidified air: I. Drying kinetics and product recovery. Dry Technol 26(6): 714–725

Gutiérrez G, Ordorica C, Osorio G, Hernández A, Patiño R, Jiménez A, Santiago T (1997) ASCON-programa para el establecimiento de las condiciones de operación en secadores por aspersión de disco rotatorio. In: Mulet A, Ordorica C, Benedito J (eds) Herramientas de cálculo en ingeniería de alimentos III. Univ. Politécnica de Valencia, Instituto Politécnico Nacional, España-México, pp 93–103

Gutiérrez G, Osorio G, Jiménez A, Pyle L (1998) An assessment of droplet-air contact and spray drying performance in bioprocess engineering. In: Galindo E, Ramírez O (eds) Advances in bioprocess engineering II. Kluwer, The Netherlands, pp 251–275

Hecht J, King C (2000) Spray drying: influence of developing drop morphology on drying rates and retention of volatile substances. 1. Single-drop experiments. Indus Eng Chem Res 39:1756–1765

Huang L, Passos M, Kumar K, Mujumdar A (2005) A three-dimensional simulation of a spray dryer fitted with a rotary atomizer. Dry Technol 23(9–11):1859–1873

Langrish T, Williams J, Fletcher D (2004) Simulation of the effects of inlet swirl on gas flow patterns in a pilot-scale spray dryer. Chem Eng Res Des 82(7):821–833

McCormick P (1962) Gas velocity effects on heat transfer in direct heat rotary dryers. Chem Eng Prog 58(6):57–61

Mujumdar A, Devahastin S (2000) Mujumdar's practical guide to industrial drying. Exergex Corporation, Canada

Oakley D (1994) Scale-up of spray dryers with the aid of computational fluid dynamics. Dry Technol 12(1–2):217–233

Seydel P, Blömer J, Bertling J (2006) Modeling particle formation at spray drying using population balances. Dry Technol 24(2):137–146

Southwell D, Langrish T (2000) Observations of flow patterns in a spray dryer. Dry Technol 18(3):661–685

Treybal R (1996) Mass transfer operations. McGraw-Hill, México

Van den Bleek C, Coppens M-O, Schouten J (2002) Application of chaos analysis to multiphase reactors. Chem Eng Sci 57(22–23):4763–4778

Wolf A, Swift J, Swinney H, Vastano J (1985) Determining Lyapunov exponents from a time series. Physica D 16(3):285–317

Zbicinski I, Li X (2006) Conditions for accurate CFD modeling of spray-drying process. Dry Technol 24(9):1109–1114

Zbicinski I, Delag A, Strumillo C, Adamiec J (2002) Advanced experimental analysis of drying kinetics in spray drying. Chem Eng J 28:207–216